SWAP Calibration Information

This document describes the calibration incorporated into the data pipeline (level 3), and information included in the SWAP calibration directory, which is necessary for further data processing (level 4 and higher). Currently, the pipeline includes calibration information to perform the background subtraction for all plan 0 and plan 3 measurements, and to calculate the energy labels for the spectrograms. The energy bins were calculated using an instrument model, which combined all the calibration information discussed in this document. Since the energy bins were calculated assuming ions entered the instrument in the center of the instrument, and the energy does not depend on some quantities such as the geometric factor, the energy bin calculations are primarily a function of the RPA and ESA response curves. The additional information discussed required for further data processing include: the instrument field of view, angular responses of the RPA and ESA, deflector calibration, and geometric factor. Much of the calibration data is discussed in the SWAP instrument paper, the instrument paper is included in the document directory in the file swap_ssr.pdf. We refer to some figures in the instrument paper, and provide some further details necessary to work with our data. We refer to some figures in the instrument paper [MCCOMASETAL2008]. This paper is the file swap_ssr.pdf.

1) Retarding Potential Analyzer (RPA)

Figure 1 shows the general shape of the RPA response over the full voltage range. Normalized coincidence is plotted as a function of the RPA voltage/beam energy. Because the individual RPA grids have a finite thickness, they act as a series of electrostatic lenses. The features in this figure, including maximum near 0.945, are due to the focusing properties.

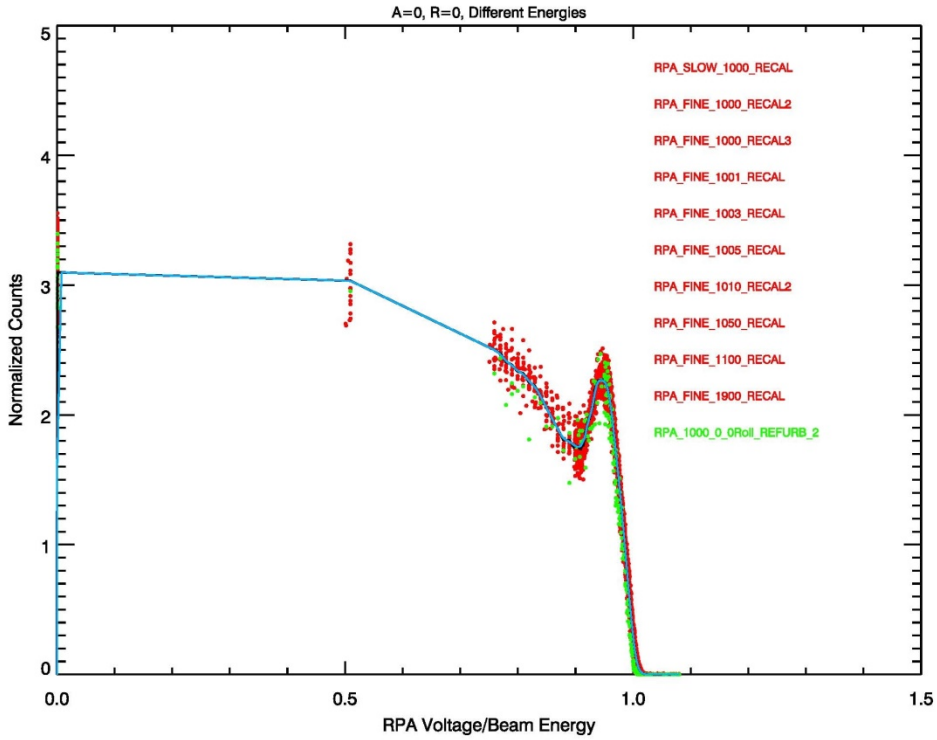

Figure 1. General shape of RPA response over full voltage range

2) Deflector System (DFL)

The nominal FOV of the SWAP instrument is 276° about the spacecraft roll axis by 10° in the plane normal to the roll axis. SWAP uses an electrostatic deflection (DFL) plate to increase the FOV out of plane by up to 15° in azimuth (α) (range is 0 to 15°). The required DFL voltage, normalized to the beam energy goes as

(1)

where ↣ is the angle from the plane.

For non-normal incident particles, the RPA response needs a calibration correction. For an ideal RPA, non-normal incident particles with $E/q > (V_{RPA} / \cos^2 \alpha$ would be passed. The unique focusing properties of the SWAP RPA lead to a more complicated response function. Figure 2 shows the normalized response of the RPA as a function of the azimuth angle. The RPA voltage is scaled by the incident beam energy. Protons with energy of

1000, 1010, and 1900 eV are shown in red, green and blue, respectively. We set the DFL voltage according to Equation 1, leading to an empirically derived calibration function for SWAP:

(2)

For the SWAP RPA, non-normal incident particles with E/q > (V_{RPA} / f(Ω)) would be passed.

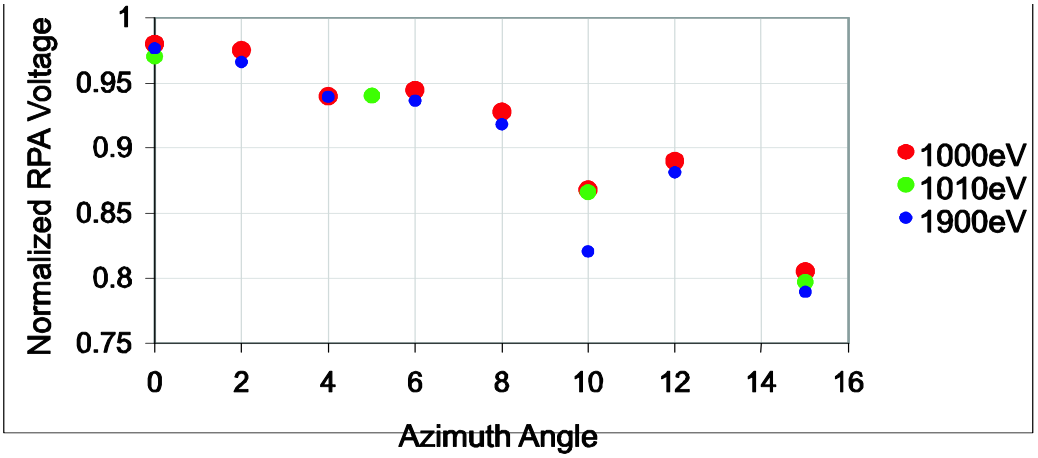

Figure 2. Normalized response of RPA as a function of azimuth angle

3) Electrostatic Analyzer (ESA)

Figure 3 shows an example of the energy-angle response of the ESA to a 1keV proton beam. The RPA and deflector system′s voltages were at zero for the data shown here. For this ESA, the analyzer constant is 1.88, the energy resolution ΔE/E is 8.5%, and the angular FOV, undeflected, is 10°.

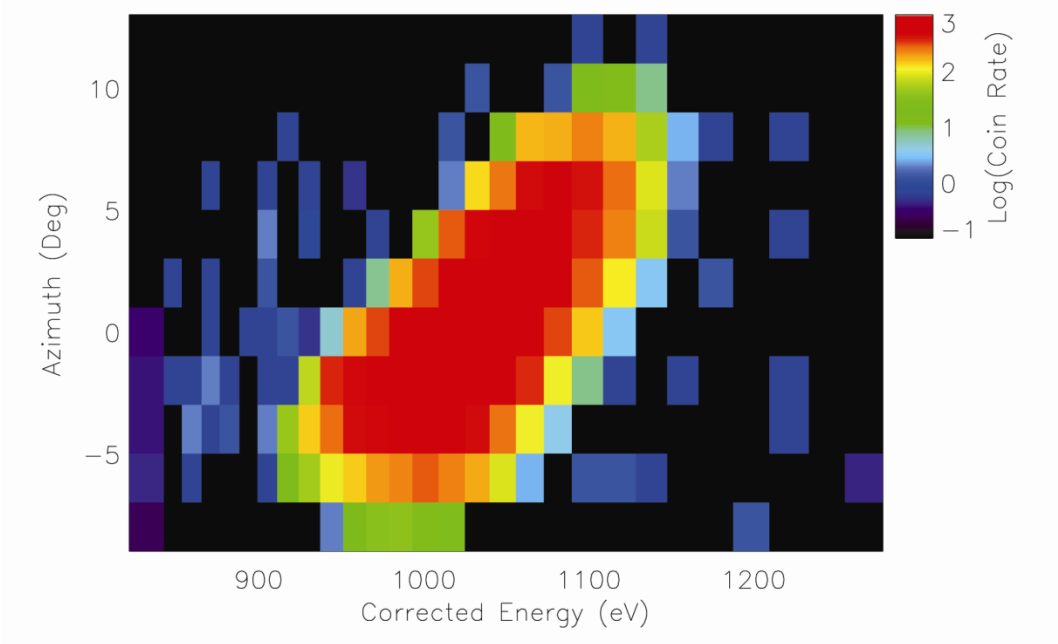

Figure 3. Example of calibration data

In addition to performing the coarse energy measurement, the ESA also blocks out UV light to the detectors. A Krypton line source, with emission at 123.6 nm and approximately the same intensity of the Sun at 1 AU, was used to test SWAP for light leaks. We used this worst-case test since SWAP operates further out in the heliosphere where the UV flux is lower by a factor of R^2. For all angles tested with the UV source, the count rate never exceeded 1 Hz for either primary or secondary rates, and no coincidence events were observed. The ESA pass band is shown in Figure 4.

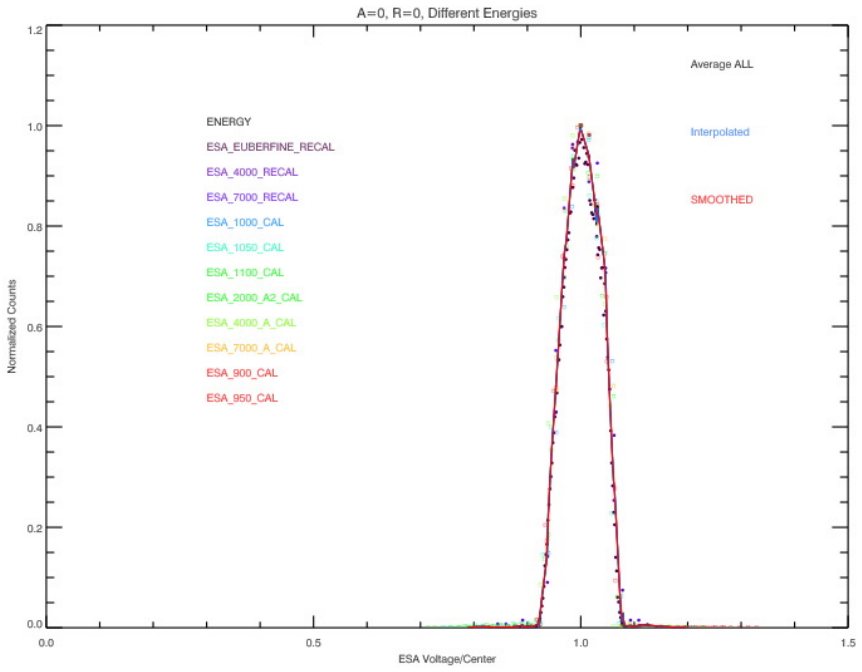

Figure 4: ESA Response function: Normalized counts versus ESA voltage normalized by the ESA voltage at the peak response.

The ESA width varies with azimuth angle. We fit many ESA response curves taken at different energies and azimuth angles, and found the full width at half max as a function of azimuth angle. We then normalized the widths by the ESA voltage (center of the ESA response) and averaged over many tests taken at different energies. Below we show these averages plotted as a function of azimuth angle (Figure 5), and we show the results in tabular form in Table 1.

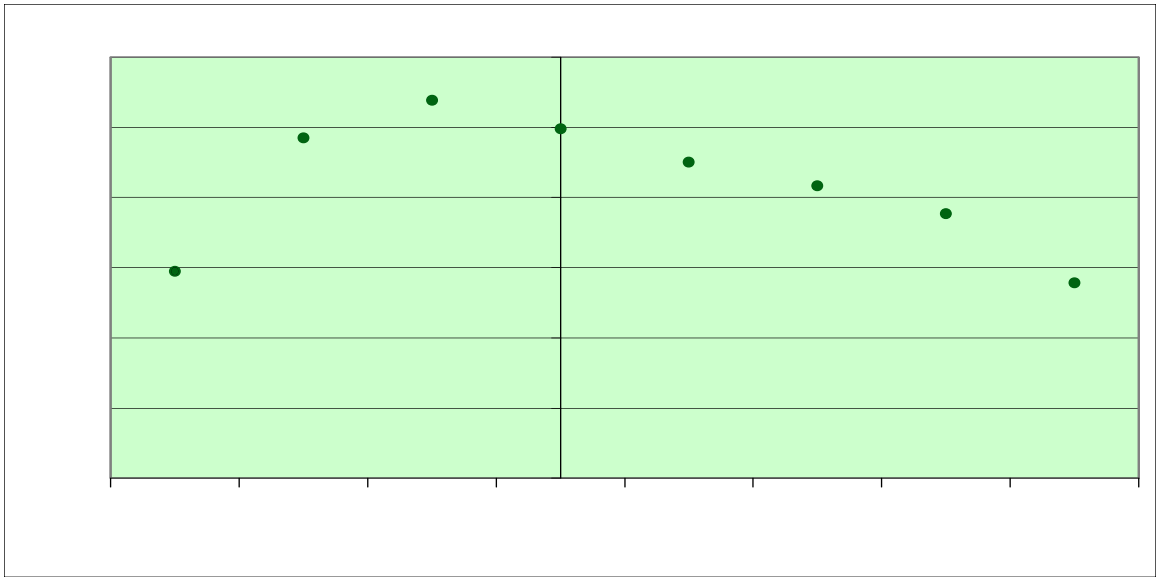

Figure 5: Ratio of the ESA response width normalized by the center of the ESA response as a function of azimuth angle.

Table 1: Normalized ESA width versus azimuth angle.

@6 E/E	Azimuth
0.0588	-6
0.0970	-4
0.1077	-2
0.0995	0
0.0900	2
0.0833	4
0.0754	6
0.0556	8

We determine the k-factor, which is the ratio between the ESA voltage and the beam energy, by examining the ratio of the ESA voltage to the beam energy at different azimuth

and roll angles (Figure 6). The k-factor was found to be a linear function of the azimuth angle (k=b+m Ω where b are the intercepts and m are the slopes), but different linear responses are observed at different roll angles. Below is a table of slopes and intercepts a different roll angles.

Table 2: Table of Slope and intercept for Varying Roll Angles

Roll Angle	m (@6 <0)	b(@6 <0)	m (@6 >0)	b(@6 >0)
-90	-0.0010849	0.538471	-0.00477399	0.537755
0	0.00036525	0.530168	-0.00489876	0.527318
90	-0.000227406	0.529935	-0.00491875	0.528725

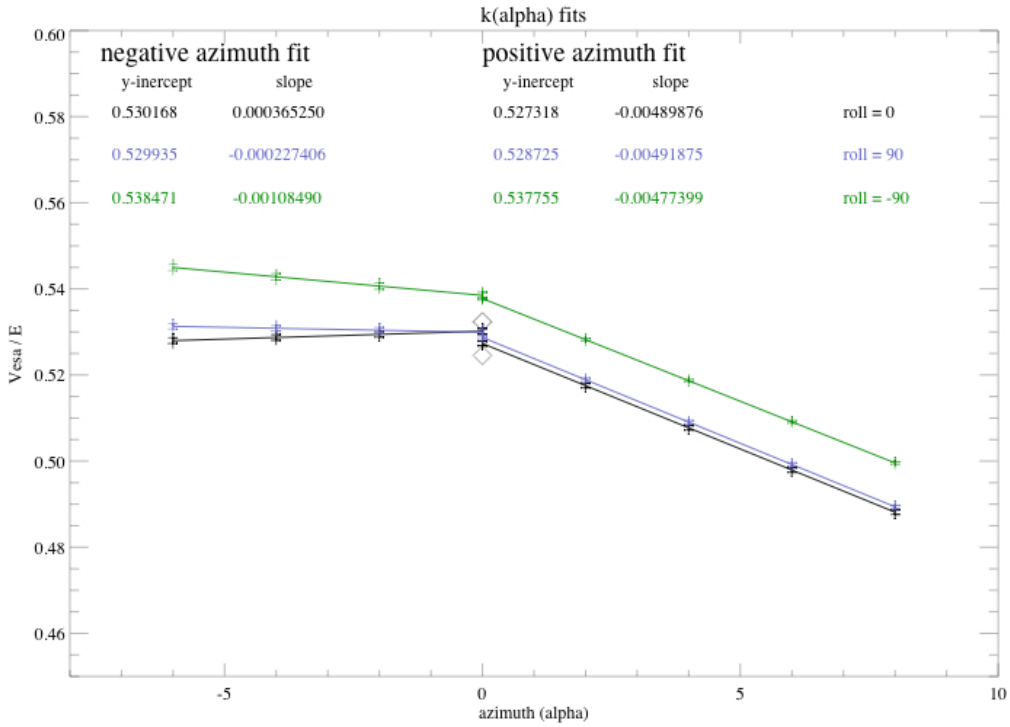

Figure 6: The ratio of the ESA voltage to the beam energy at different azimuth and roll angles.

4) Energy Bin Calculations

The location of the energy bin peak response is calculated using the instrument model, which is based on many different functions and parameters determined in the calibration. The energy bin peak response depends on the voltage settings of the RPA, ESA, DFL and the angle at which the ions enter. For science observations in the Jupiter phase, the deflector voltage was zero except during the angle test. Since we do not know the angle at which the ions enter, we assume the ions enter the center of the instrument; this assumption limits the uncertainty in the location of the center of the ESA passband to about 10% for ions entering anywhere in the 10° instrument Field-Of-View (see Figure 31 of [MCCOMASETAL2008]). We then use the RPA and ESA voltage setting to calculate the center of the combined response. We have the energy of the peak response for each RPA and ESA voltage setting in the onboard voltage tables. In the calibration directory we list the filenames of the precalculated energy bin centers and the time periods over which they are valid in the list_energy_files.tab file. Each energy bin file (i.e., esa_rpa_v19_energy_binsf.csv, filename suffix extension is .tab in PDS data sets) lists the plan number, sweep, number, ESA DAC, RPA DAC, ESA voltage, RPA voltage, the crossing ratio (ratio of the RPA voltage to the ESA center energy), energy at the peak response, energy width (FWHM), minimum energy, and maximum energy. These energy tables are used to determine the energy in the spectrograms.

5) Detectors

Ions that pass through the sensor then pass through a thin carbon foil and are measured by the PCEM. Secondary electrons liberated from the carbon foil are attracted to the SCEM. Events that are measured by both the PCEM and SCEM within 100 nanoseconds of time are recorded as coincidence (COIN) events.

We determined the operation voltage for PCEM and SCEM by sweeping the voltage while illuminating the instrument with a constant intensity 1 keV proton source. Figure 7 shows the response of the PCEM, SCEM, and the COIN rate as a function of voltage. For the data shown here, the voltage applied to the PCEM and SCEM were equal. From these tests, we selected a nominal operation voltage of 2100 V at start of mission, which is well into the

saturation region of the CEM gain curves. The high voltage power supplies for the CEMs were designed to output up to 4.5 kV, allowing us to increase the voltage to the CEMs if their gain degrades over the mission lifetime.

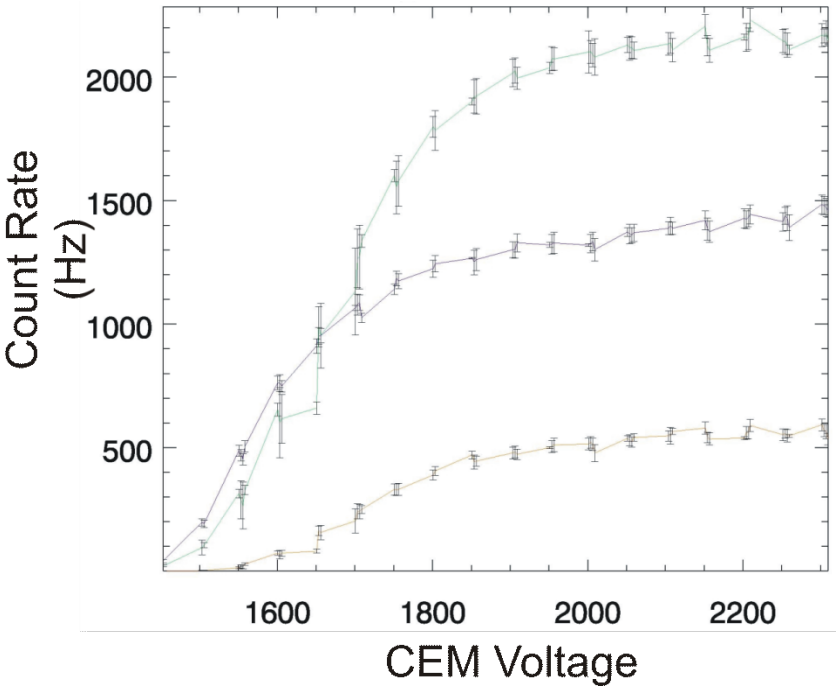

Figure 7. PCEM, SCEM, and coincidence rate response as a function of voltage.

In the table below we list the effective areas and geometric factors for the PCEM, SCEM, coincidence and a combined detection in the PCEM, SCEM, or coincidence.

Table 3: Effective Area and Geometric Factor

Detection Signal	Geometric Factor	Effective Area
PCEM	4.1e-3 cm^2 sr eV/eV	0.058 cm^2
SCEM	8.6e-3 cm^2 sr eV/eV	0.12 cm^2
Coincidence	1.8e-3 cm^2 sr eV/eV	0.025 cm^2
Any detection	1.1e-2 cm^2 sr eV/eV	0.15 cm^2

5) Field of View (FOV):

In order to determine the field of view of the ESA, the RPA is turned off and the beam was fixed at one energy, and then the beam was moved to different roll and azimuth angles. The counts are recorded at each roll and azimuth setting until the full field of view of the instrument was covered at 1.0 degree resolution. The result is a 2-D array of counts in roll and azimuth. Below we show this array normalized by the maximum count rate in the array (Figure 8).

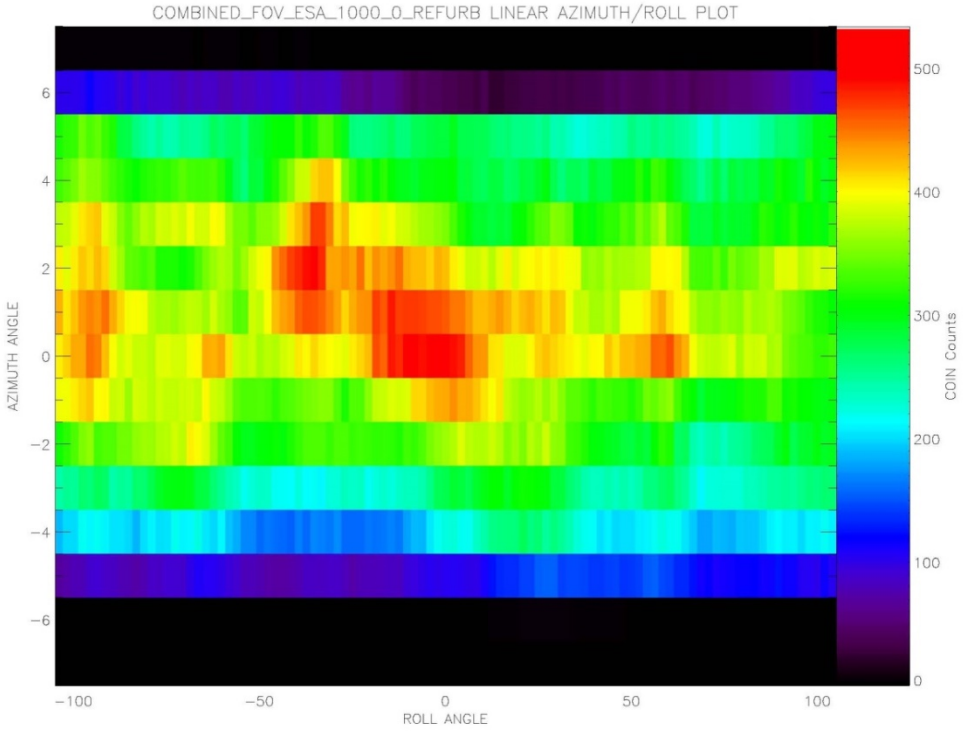

Figure 8: Field of View of the ESA: Normalized counts in color as a function of roll and azimuth.

7) *Background Subtraction*

When the RPA is operating there is a background that needs to be removed. During the Jupiter phase we use plan 0/sweep 0 and plan 5/sweep 5 where the plans and sweeps refer to the RPA and ESA voltage tables. In plan 5 we do not use the RPA; consequently, there is no background to remove. In plan 0 we do need to remove the background. The background varies with the distance to the Sun. The current background files are based

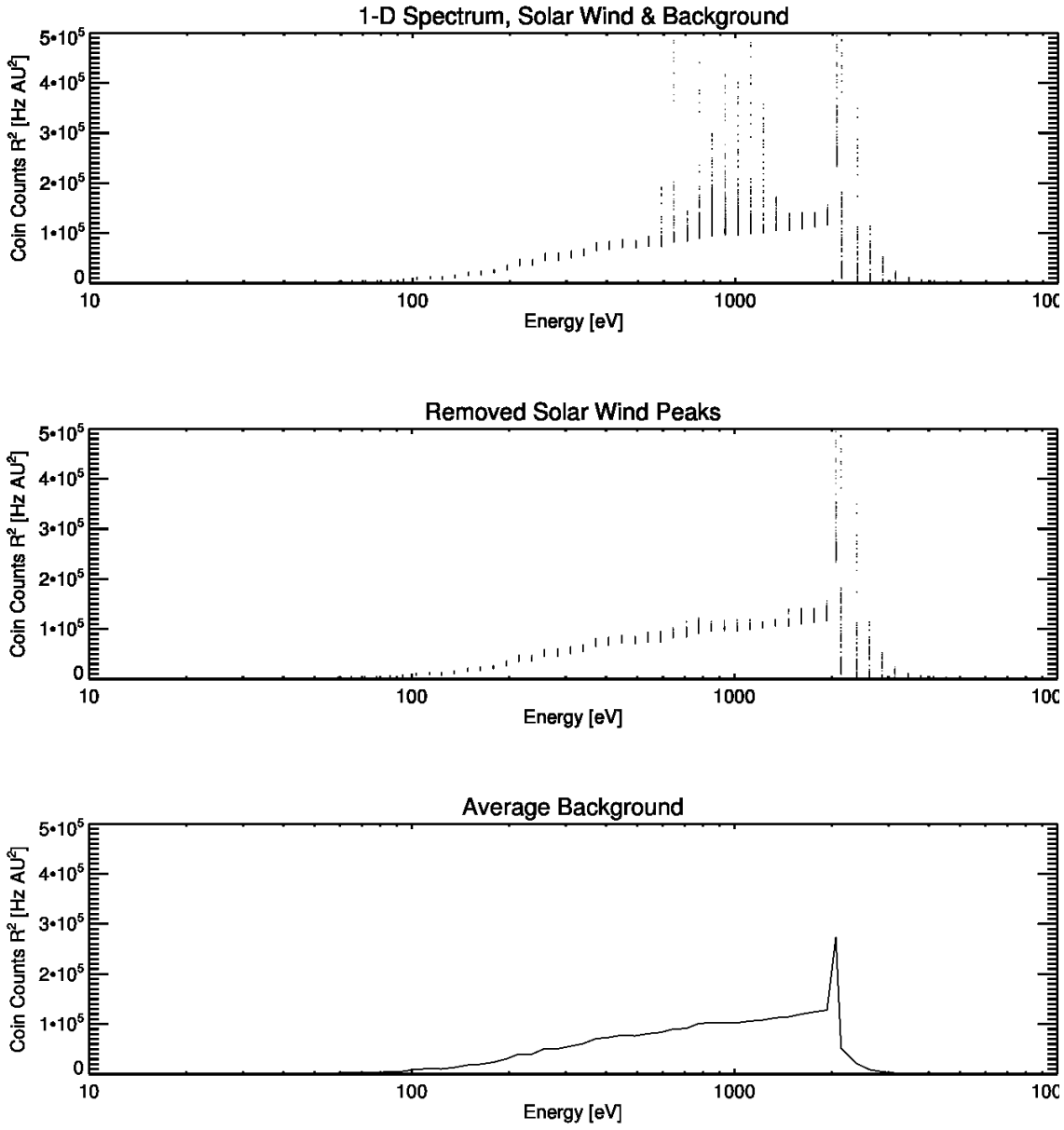

Figure 9: *In the top panel the SWAP-009-6 coincidence count rates in Hz times the distances from the Sun, in AU, squared are shown as a function of energy. The middle panel is the same data with the spikes removed. The data is then binned and averaged (bottom panel).*

on calibration measurements taken during the sequence SWAP-009-6. In Figure 9 we show the SWAP-009-6 data for days 290-292, 299-301, 304-309, 316-318, 320-321, 335-339, 343- 344 used to create the background files. Here we plot the count rates in Hz times the square of the distance from the Sun in AU ($R_{Sun,AU}$) versus the energy. Most of the vertical spikes are the solar wind peaks. In the middle panel the solar wind peak and 3 points below and above the energy of the peak have been removed from each scan individually. The bottom panel of Figure 9 is an average of the top bin where the average has been performed on each bin individually since there are a different number of data points in each bin after removing the solar wind peaks.

To use the background information in the pipeline the data was converted from Hz back to counts/sample since the background subtraction is done prior to the rest of the data processing. The background rates (counts / sample) are scaled by the square of the distance to the Sun ($R_{Sun,AU}$) and those scaled rates (counts * $(R_{Sun,AU})^2$ / sample) are stored in the background files in the calibration directory. To remove the background we first scale the measured count rates by the distance to the Sun squared, and then subtract scaled background rates. After the subtraction the result is then divided by the distance to the Sun squared to obtain the rates in units of counts per sample. The background filenames and the time range for each file are listed in the list_background_files.tab file. The background file used during the Jupiter phase is called background_009_dac_jup.tab. The background files contain the peak energy, ESA DAC, RPA DAC, PCEM background, SCEM background, and coincidence background rates in counts * $(R_{Sun,AU})^2$ / sample .

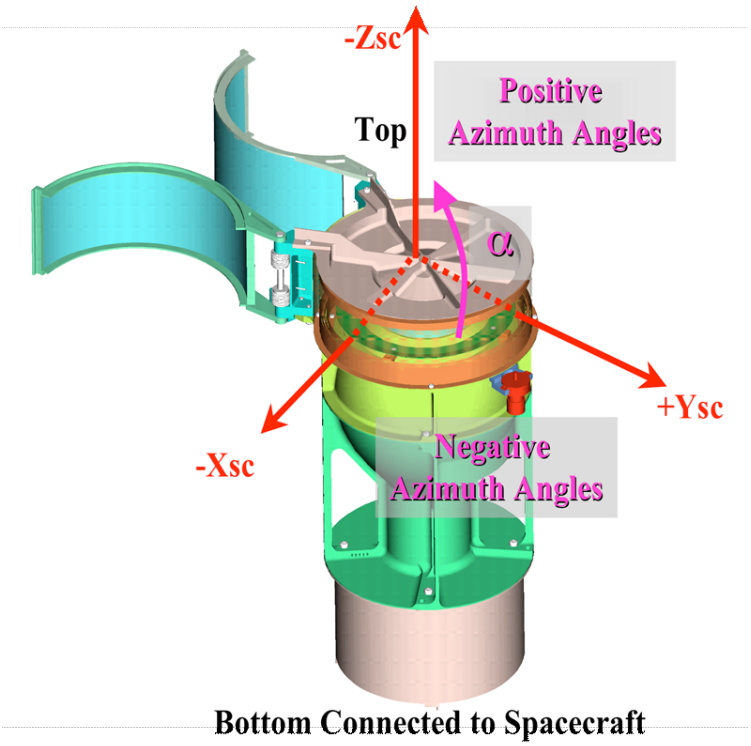

Figure 10: Diagram defining the azimuth angle. Bottom of the instrument connects to the spacecraft.

The RPA response also depends on the azimuth (α) angle that the ions enter the instrument. Figure 10 defines the azimuth angle to be positive towards the top of the instrument and negative toward the bottom of the instrument. Ideally, non-normal incident particles with $E/q > (V_{RPA} / \cos^2\alpha)$ would be passed; however, the focusing properties of the SWAP RPA lead to a more complex response function. In Figure 30 of the instrument paper the normalized response of the RPA as a function of the azimuth angle is shown.

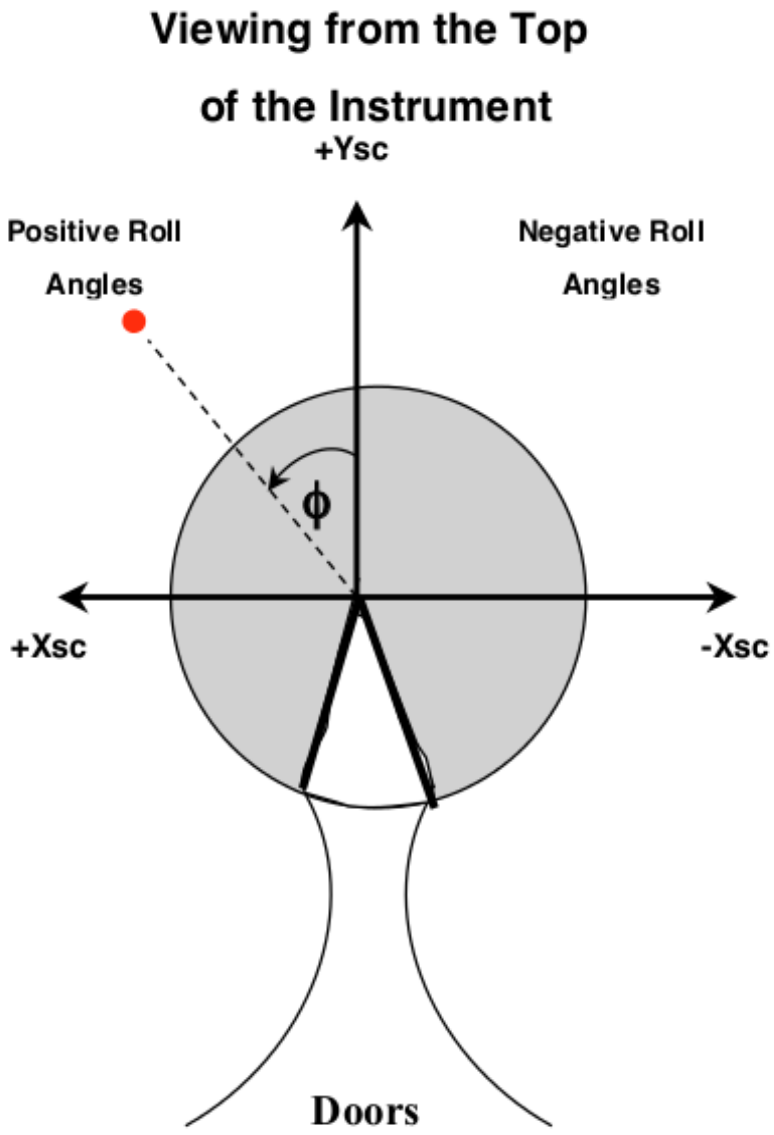

Figure 11: Definition of the Roll Angle

Looking down on the top of the instrument the roll (φ) angle is in the X-Y spacecraft plane with positive roll angles towards the +Xsc axis and the negative roll angles towards the −Xsc axis (Figure 11).